A topological point defect regulates the evolution of extended defects in irradiated silicon

Hyoungki Park[a] and John W. Wilkins
Department of Physics, The Ohio State University, Columbus, Ohio 43210, USA

(Received 14 February 2011; accepted 8 April 2011; published online 29 April 2011)

Clustering and annihilation of atomic-scale bond defects dominate nucleation and evolution of submicron-scale extended interstitial defects in irradiated silicon. Molecular dynamics simulations reveal the role of the bond defect in the thermal evolution of extended defects and identify the atomistic evolution paths. Accurate density functional theory calculations establish formation energies, activation barriers, and electronic structures of the bond defect and its clusters, and extended interstitial defects. © *2011 American Institute of Physics*. [doi:10.1063/1.3585656]

Knowledge of the microscopic processes of nucleation, evolution, and annihilation of defects is essential for understanding and controlling changes in material properties. A topological point defect, the Stone–Wales defect,[1] has important implications for mechanical, electronic, and transport properties of carbon and other sp^2-bonded nanostructures.[2] The similar topological defect, the bond defect, is generated by irradiation for the diamond-phase Si.[3–7] Here, we use the classical molecular dynamics (MD) simulations with a modified embedded atom method potential[8] and density functional theory (DFT) calculations with the Heyd–Scuseria–Ernzerhof (HSE) hybrid functional[9] to study the role of bond defect in the formation and evolution of three extended interstitial defects[10–12] observed during the thermal treatment of the irradiated Si. Despite decade-long experimental observations,[11,13–15] understanding atomistic mechanism of their formation and thermal evolution has been elusive. We show that bond defect is the key structural element of extended defects, and the thermally triggered cascade of atomic-scale annihilation of bond defects drives the submicron-scale complex structural evolution of extended defects.

Figure 1 shows the atomic structure of the bond defect in Si, a topological point defect characterized by a rotated pair of lattice atoms around their bond center and the associated altered local bonding structure.[3–7] This defect introduces five- and seven-member rings in the six-member ring bonding structure characteristic of diamond-phase lattice from the ⟨011⟩ perspective—the perpendicular direction to the plane of paper in all the atomic structure figures of this work. The rotation of two atoms of the deformed bond in the {011} plane back to crystalline positions annihilates the defect.

Table I lists results of large-scale DFT calculations with the HSE functional showing that the formation energy of an *isolated single* bond defect is 2.95 eV, which is comparable to the energies of typical point defects in Si.[6] Furthermore, as more bond defects are stacked along ⟨011⟩, i.e., in/out of paper in Fig. 1, the structure become more stable, and a long chain has a lower formation energy per defect by about 1 eV. The calculated energy gap of the *isolated single* bond defect between the highest occupied molecular orbital (HOMO) and the lowest unoccupied molecular orbital (LUMO) is 1.14 eV, which is only 0.01 eV smaller than the calculated gap of bulk Si. Even the extended chain keeps the gap of 1.10 eV, supporting that maintaining the fourfold coordination with no excess or deficit of atoms induces only mild disturbance of the electronic structure. Compared to the experimental gap of 1.16 eV for bulk Si,[16] the calculated HSE gap, 1.15 eV, shows significant improvement over the Perdew–Burke–Ernzerhof (PBE) (Ref. 17) gap of 0.58 eV. This difference in their gap estimation between HSE and PBE is persistent across all the defects listed in Table I.

The height of the transition-energy barrier from a bond defect to the bulk structure is directly related to the thermal stability of the defect. The calculated barrier for an isolated single bond defect is 0.69 eV. Similar to the formation energy, the barrier is affected by the proximity of other bond defects. Figure 2 schematically displays transition barriers of ⟨011⟩ chains of bond defects. The annihilation barrier of the chain is 1.50 eV, which is 0.81 eV higher than the barrier of the isolated single bond defect. On the other hand, the barriers from the bulk to the defected structures are 3.64 and 3.44 eV for a bond defect and a defect chain, respectively, implying that the spontaneous thermal generation of those defects from the undamaged lattice is unlikely. Moreover, the annihilation barrier of 1.28 eV for one of the chains of the compound defect consisting of two adjacent bond defect chains indicates that the structures with multiple chains are also stable. As described in a classical MD study,[18] rows of bond defect chains in the {311} plane can be considered as the scaffold for {311} defects. The structure (b) in Fig. 2 shows such a structure with two bond defect chains. Adding an additional defect to either $[2\bar{3}\bar{3}]$ or $[\bar{2}33]$ side of a single

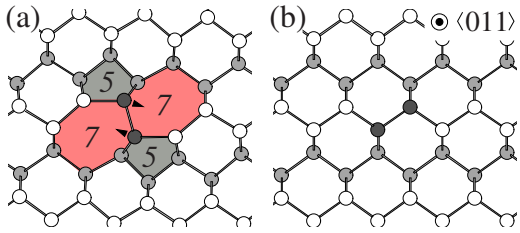

FIG. 1. (Color online) The bond defect and its annihilation: (a) the atomic configuration of a bond defect and (b) bulk. The repeating bilayer plane along ⟨011⟩ represented by white and gray atoms displays the hexagonal bonding structure. For ease of viewing the rotated atom-pair is colored in black.

[a]Electronic mail: hkpark@mps.ohio-state.edu.

TABLE I. Formation energies per defect, E_f, and HOMO-LUMO gaps, E_g, for a single, two, and three bond defects parallelly embedded along ⟨011⟩ in bulk Si, and the infinite chain of bond defect.

	E_f (eV)		E_g (eV)	
Structure	HSE	PBE	HSE	PBE
Bulk	0.00	0.00	1.15	0.58
Single defect	2.95	2.58	1.14	0.56
Two defects	2.62	2.32	1.13	0.55
Three defects	2.44	2.18	1.10	0.53
Defect chain (infinite)	1.94	1.79	1.10	0.52

defect in the figure gives rise to an eight-member ring connecting two defects in the middle, i.e., from (a) to (b) in Fig. 2. Repeating this procedure generates more eight-member rings on {311} habit planes. The ⟨011⟩ chains of this structure with di-interstitials held in some of eight-member rings become {311} defects.

Figure 3 shows the three extended interstitial defects that form during annealing of ion-implanted Si: the {311} and the {111} defect, and the Frank loop. As described in the previous paragraph, the contiguous arrangement of ⟨011⟩ bond defect chains on {311} planes generates eight-member rings that have spatial room to accommodate interstitial chains. When filled with an interstitial chain, the eight-member ring and two nearby six-member rings turn into the "*I* unit," one of the basic units used by Kohyama and Takeda[19] to explain structures of {311} defects. In their notation, the *I* unit is an interstitial chain surrounded by two seven- and two six-member rings, *O* denotes the eight-member ring, and *E* for seven-member rings at the defect boundaries. Using the notation the {311} defect of Fig. 3(a) can be represented as *EIIOIIE*. Depending on the number of *I* and *O* units, and the sequence of their arrangement between *E* units, defects have different formation energies.[20]

Figure 3(b) displays a previously proposed structural model for the {111} defect,[21] and Fig. 3(c) is the structure of the Frank loop whose interstitial chains are all connected and form a piece of faulted interstitial plane. Both {111} defects and Frank loops have the same habit planes for their interstitial chains, {111}. As in the {311} defect, eight-member rings of the {111} defect structure can hold additional interstitial chains. If all the eight-member rings of the {111} defect are filled with interstitial chains, the structure becomes a Frank loop. Hence, we believe that the {111} defect is the intermediate structure during the transformation of {311} defects with "unfilled" eight-member rings to Frank loops. This view is consistent with an experimental[11] observation and results of our MD simulations.[20] Unlike {311} defects, Frank loops have much reduced local-electronic-gaps of about 0.3 eV. Again, PBE greatly underestimates gaps, predicting all Frank loops to be metallic.

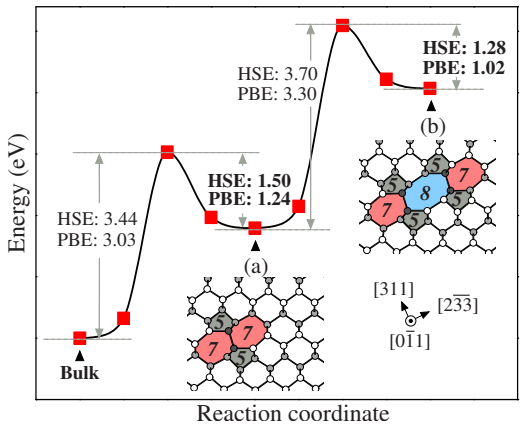

FIG. 2. (Color online) Transition barriers of (a) a bond defect chain running along $[0\bar{1}1]$, and (b) a compound defect consisting of two adjacent bond defect chains in $[2\bar{3}\bar{3}]$ direction. In (b), the rotation of either one of two pairs of atoms in black annihilate one bond defect chain and transforms the structure to (a).

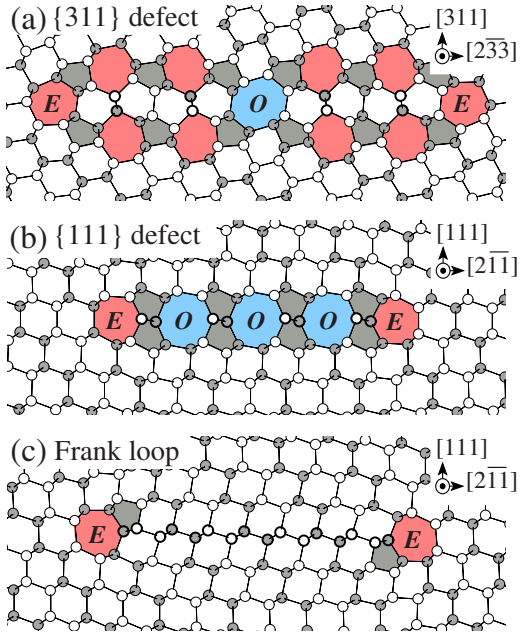

FIG. 3. (Color online) The atomic configurations of extended interstitial defects in the $(0\bar{1}1)$ bilayer plane. A pair of white and gray interstitial atoms in bold circles represents the repeating unit of an interstitial chain running in/out of paper: four interstitial chains are depicted in (a) and (b), eight chains in (c). In each figure, the end-units *E*s set the width of the defect by forming boundaries between defects and bulk Si.

Formation energies of three extended defects of our HSE calculations[20] closely agree with previous results.[20,12,21] The calculated formation energy hierarchy among three types of extended defects indicates that the formation of the {311} defect is initially favored during the annealing of an irradiated sample. Subsequently, {311} defects can evolve into Frank loops. Figure 4 demonstrates a thermally activated transition path from a {311} defect to a Frank loop analyzed on one of $(0\bar{1}1)$ bilayer planes comprising these defects.

Our extensive classical MD simulations identify that the same rotation of a pair of neighboring atoms that annihilates the bond defect converts a "seven+five"-member ring of {311} defects into six-member rings, and drives the transformation to the Frank loop. In Fig. 4(a), the rotation of the first pair moves the "seven+five"-member ring to the adjacent position, and changes the local bonding structure for the second pair in Fig. 4(b) to be same as the bond defect. The rotation of the second pair in Fig. 4(b) converts two "seven+five"-member rings into four six-member ring. This two-step process continues until all "seven+five"-member rings but end-units are converted into six-member rings. In other words, the annihilation process of bond defects that serves as

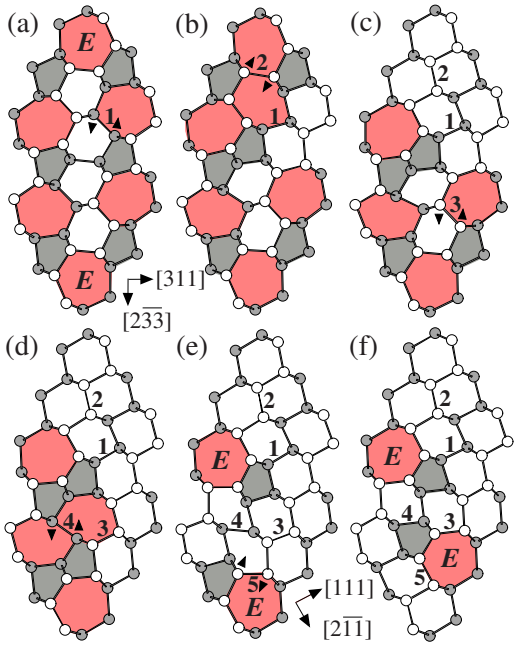

FIG. 4. (Color online) Schematic presentation of one of transformation paths from the {311} *EIIE* defect to the Frank loop with two interstitial chains in a (0$\bar{1}$1) bilayer plane, (a) to (e). (e) to (f) is an extra step making the Frank loop more stable by aligning two end-units. Rotating pairs are sequentially indexed by evolution stages, 1-2-3-4-5. Following different sequences are also possible. The number of feasible paths grows rapidly with increasing temperature and number of interstitial chains in {311} defects. However, the key mechanism is same for all transformation paths.

the scaffold of {311} defects is the key mechanism of the transformation. The cascade of annihilation process is thermally triggered with reaction barriers of about 1.5–2.4 eV depending on the evolution stages and local structures.[20] The transformation can progress coherently across many (0$\bar{1}$1) bilayer planes but at high temperatures, the coherency is greatly disrupted and multiple Frank loops can evolve from a long {311} defect.

In conclusion, the bond defect has the comparable formation energy to the energies of typical point defects in irradiated Si, and is stable enough to participate in formation of extended defects during the thermal treatment. Clustering of bond defects generates anomalous local bonding patterns. The bond defect is the key structural element of {311} defects. During annealing, the annihilation of bond defects in {311} defects is thermally triggered and drive the transformation into Frank loops. Additionally, the critical role of the bond defect in the thermal evolution of {311} defects implies its possible participation in the formation of the small precursor clusters that grow into {311} defects. Studying small interstitial clusters with bond defects may deepen our understanding of structures and energetics of those precursors that are experimentally observed.[22]

HSE hybrid functional and the projector augmented wave method[23,24] with the plane-wave cutoff of 300 eV is used as implemented in the Vienna *ab initio* simulation package (VASP).[25,26] The isolated bond defects are modeled in 980 atom supercells with $7\times a_0/\sqrt{2}$ along [011], $5\times a_0$ along [100], and $7\times a_0/\sqrt{2}$ along [01$\bar{1}$], where a_0=5.435 Å. The lattice constant is chosen to be optimal for the HSE functional.[27] On the other hand, the bond defect chains and extended interstitial defects are modeled to periodically repeat in [01$\bar{1}$] direction with two atomic layers. The resulting bilayer has $15\times a_0/\sqrt{2}$ along [011], $7\times a_0$ along [100], and $a_0/\sqrt{2}$ along [01$\bar{1}$]. The supercells contain 420 bulk atoms and interstitials, and $1\times1\times16$ k-point mesh is used. The climbing-image nudged elastic band (Ref. 28) with the perpendicular force convergence criterion of <1 meV/Å computes transition barriers for the bond defect. The MD simulations with more than 16 000 atoms run more than 20 ns with 1 fs time-step at the temperature range from 1100 to 1400 K.

This work was supported by DOE-BES-DMS (Grant No. DE-FG02-99ER45795). Computational resources were provided by the National Energy Research Scientific Computing Center, supported by the Office of Science of the U.S. Department of Energy (Grant No. DE-AC02-05CH11231), and the Ohio Supercomputer Center.

[1] A. J. Stone and D. J. Wales, Chem. Phys. Lett. **128**, 501 (1986).
[2] A. V. Krasheninnikov and K. Nordlund, J. Appl. Phys. **107**, 071301 (2010), and references therein.
[3] M. Tang, L. Colombo, J. Zhu, and T. Diaz de la Rubia, Phys. Rev. B **55**, 14279 (1997).
[4] D. M. Stock, B. Weber, and K. Gärtner, Phys. Rev. B **61**, 8150 (2000).
[5] F. Cargnoni, C. Gatti, and L. Colombo, Phys. Rev. B **57**, 170 (1998).
[6] S. Goedecker, T. Deutsch, and L. Billard, Phys. Rev. Lett. **88**, 235501 (2002).
[7] O. K. Al-Mushadani and R. J. Needs, Phys. Rev. B **68**, 235205 (2003).
[8] S. A. Ghasemi, M. Amsler, R. G. Hennig, S. Roy, S. Goedecker, T. J. Lenosky, C. J. Umrigar, L. Genovese, T. Morishita, and K. Nishio, Phys. Rev. B **81**, 214107 (2010), and references therein.
[9] J. Heyd, G. E. Scuseria, and M. Ernzerhof, J. Chem. Phys. **118**, 8207 (2003); **124**, 219906 (2006).
[10] A. Claverie, B. Colombeau, B. De Mauduit, C. Bonafos, X. Hebras, G. Ben Assayag, and F. Cristiano, Appl. Phys. A: Mater. Sci. Process. **76**, 1025 (2003).
[11] S. Boninelli, N. Cherkashin, A. Claverie, and F. Cristiano, Appl. Phys. Lett. **89**, 161904 (2006).
[12] H. Park and J. W. Wilkins, Phys. Rev. B **79**, 241203 (2009).
[13] D. J. Eaglesham, P. A. Stolk, H. J. Gossmann, T. E. Haynes, and J. M. Poate, Nucl. Instrum. Methods Phys. Res. B **106**, 191 (1995).
[14] L. S. Robertson, K. S. Jones, L. M. Rubin, and J. Jackson, J. Appl. Phys. **87**, 2910 (2000).
[15] G. Z. Pan, R. P. Ostroumov, L. P. Ren, Y. G. Lian, and K. L. Wang, J. Non-Cryst. Solids **352**, 2506 (2006).
[16] H. M. Sze, *The Physics of Simiconductor Devices* (Wiley, New York, 1969).
[17] J. P. Perdew, K. Burke, and M. Ernzerhof, Phys. Rev. Lett. **77**, 3865 (1996).
[18] L. A. Marqués, L. Pelaz, I. Santos, P. López, and M. Aboy, Phys. Rev. B **78**, 193201 (2008).
[19] M. Kohyama and S. Takeda, Phys. Rev. B **46**, 12305 (1992).
[20] See supplementary material at http://dx.doi.org/10.1063/1.3585656 for the calculated formation energies and band gaps of three extended interstitial defects, the illustrated transition paths from {311} defects to Frank loops, and the calculated transition barriers.
[21] C. T. Chou, D. J. H. Cockayne, J. Zou, P. Kringhøj, and C. Jagadish, Phys. Rev. B **52**, 17223 (1995).
[22] N. E. B. Cowern, G. Mannino, P. A. Stolk, F. Roozeboom, H. G. A. Huizing, J. G. M. van Berkum, F. Cristiano, A. Claverie, and M. Jaraíz, Phys. Rev. Lett. **82**, 4460 (1999).
[23] P. E. Blöchl, Phys. Rev. B **50**, 17953 (1994).
[24] G. Kresse and D. Joubert, Phys. Rev. B **59**, 1758 (1999).
[25] G. Kresse and J. Furthmüller, Comput. Mater. Sci. **6**, 15 (1996).
[26] G. Kresse and J. Furthmüller, Phys. Rev. B **54**, 11169 (1996).
[27] K. Hummer, J. Harl, and G. Kresse, Phys. Rev. B **80**, 115205 (2009).
[28] G. Henkelman, B. P. Uberuaga, and H. Jónsson, J. Chem. Phys. **113**, 9901 (2000).